

Robust Key-Frame Stereo Visual SLAM with low-threshold Point and Line Features

Meiyu Zhi

Abstract—In this paper, we develop a robust, efficient visual SLAM system that utilizes spatial inhibition of low threshold, baseline lines, and closed-loop keyframe features. Using ORB-SLAM2, our methods include stereo matching, frame tracking, local bundle adjustment, and line and point global bundle adjustment. In particular, we contribute re-projection in line with the baseline. Fusing lines in the system consume colossal time, and we reduce the time from distributing points to utilizing spatial suppression of feature points. In addition, low threshold key points can be more effective in dealing with low textures. In order to overcome Tracking keyframe redundant problems, an efficient and robust closed-loop tracking key frame is proposed. The proposed SLAM has been extensively tested in KITTI and EuRoC datasets, demonstrating that the proposed system is superior to state-of-the-art methods in various scenarios.

Index Terms—Visual SLAM, Suppression OF Feature Low-threshold Points, Low Texture, Baseline Line, Closed-loop Keyframe.

I. INTRODUCTION

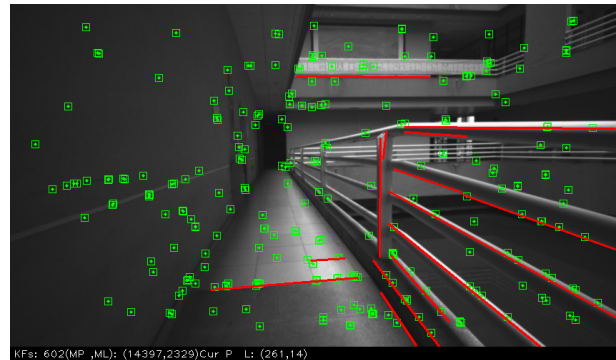
VISUAL Localization and Mapping algorithms are used to estimate the 6D camera pose while recreating unknown environments, which are critical for autonomous robots and augmented reality because camera attitude estimation enables cars and Unmanned aerial vehicles to position themselves.

VSLAM is divided into two direct methods: DSO [1] and SVO [2], and feature point methods such as ORB-SLAM2 [3]. The feature point method uses continuous frame tracking to identify key points and then recovers camera motion trajectory and 3-D points. ORB-SLAM2 is considered to be the current state-of-the-art SLAM system. It is developed based on many excellent works. e. g. , PL-SLAM [4], [5], an efficient graph-based bundle adjustment (BA) algorithm. The point-based approach is robust because the key points are invariant relative to views and illumination. Therefore, The VSLAM system screening key points to maintain robustness. The quad-tree [3] and kd-tree [6] are important data structures for screening key points to solve key points redundancy. In addition, low threshold keypoints can be more effective in dealing with low textures.

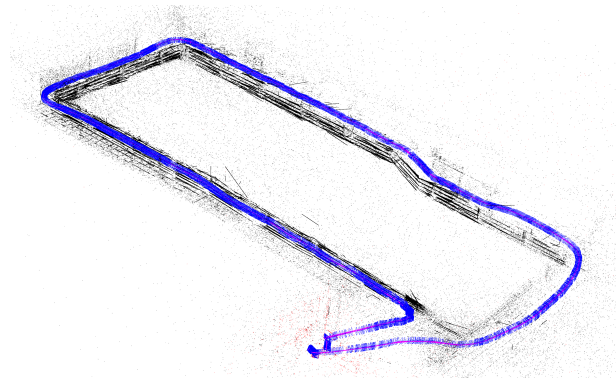
Recently, combined line features and point features have become favorable for the VSLAM due to low texture and

This work was supported in part by the National Natural Science Foundation of China under Grants (62121004, 61876041), the Local Innovative and Research Teams Project of Guangdong Special Support Program (2019BT02X353), Key Area Research and Development Program of Guangdong Province (2021B0101410005), and Guangdong Basic and Applied Basic Research Foundation (2021B1515420008).

H. Rao and Y. Xu are with the Provincial Key Laboratory of Intelligent Decision and Cooperative Control, School of Automation, Guangdong University of Technology, Guangzhou 510006, China. (e-mail: raohxia@163.com, xuyong809@163.com)



(a) Point and line features are witnessed in one image. .



(b) The point and line map

Fig. 1. The proposed visual SLAM with point and line features on our dataset. Note that in (b), the purple lines indicate the trajectory of camera motion. The blue frames represent keyframes, the current frame in red, and the local map for the Tracking at that moment in red.

adaptation to a more realistic environment such as indoor and outdoor scenes. Dealing with low texture-specific SLAM methods based on lines and points, such as S-SLAM [7], Stereo-PL-SLAM [5], [8] For reconstruction, point and line SLAM is sparse mapping. Compared to point SLAM, it has only an incomplete map. Having lines in maps improves the approximation accuracy and has 3D reconstruction on line [9]. However, small errors accumulate over time. To overcome these errors, strategies are loop-closure detection [10] and reconstruct a high accuracy map [8]. Loop closure detection, combined with pose graph optimization, detects previously seen landmarks and optimizes the pose graph based on new constraints. However, Loop closure adds an extra computational burden and removes the drift only when revisiting the same place. Another strategy is to build a global landmark in the world frame. Extracting lines by Line Segment Detec-

tor(LSD) [11] contain broke lines. Therefore, the connection disconnection can effectively improve localization precision [12].

The keyframe strategy has high accuracy for localization [3]. Keyframe extraction reduces the number of images to be processed and reduces redundant information [13]. An appropriate number of keyframes is critical for stability.

In this paper, We build on our Stereo-SLAM and propose a robust SLAM designed to deal with and adapt to various environments, including low texture, reducing time, and improving tracking and mapping simultaneously. Fig .1 presents a tracking and mapping process containing points and line segments. Different to [1], [3], [5], the baseline is merged into error line functions and line Jacobian, which improves the estimation accuracy. In summary, our contributions are:

- An improved extraction method for low-threshold points is introduced to reduce the time of the program.
- An improved extraction method for connecting broke lines is introduced to robustify data association.
- In the back-end of the proposed visual SLAM, we employ the baseline to calculate line functions and line Jacobians, which apply to frame tracking, local mapping, and global bundle adjustment.
- We design a robust keyframe strategy in which we could reasonably add keyframes to keep the system strong.

II. RELATED WORK

PTAM [14] is a monocular, keyframe-based SLAM system that was the first multithreaded system to include tracking and mapping and has been successful in real-time. As a state-of-the-art SLAM system, ORB-SLAM2 combines feature-based Tracking, sparse point Mapping, and loop closure with the Bag-of-words model. It needs to add keyframes by observation inliers between the reference frame and current frame, decreasing the quality of tracking ORB-SLAM2 insert keyframes. This method FastORB-SLAM [15] replaces ORB-SLAM2 descriptors Kanade-Lucas-Tomasi Tracking Method(KLT), which reduces match points-to-points time. Oleksandr Bailos' [16] proposes an efficient adaptive non-maximal suppression algorithm for keypoints distribution to minimize the time to finish the program. This algorithm finds a global response value more significant than the set threshold. LSD [11] is a short line segment detection to adopt a pyramid of images to determine the picture's location. Compared to THRESH-OTSU to extract the line, LSD extracted lines more accurately. LBD(Line Band Descriptor) [17] is a method describing a line of feature using a binary string which is an efficient method to match a line. XOR operations applying to Binary string improved match line-to-line.

Inspired by the LSD and LBD, PL-SLAM [4] incorporates lines which include frame tracking, local mapping, bag-of-words about line, and global BA. In addition, PL-SLAM in texture with fewer points can run steady. RPL-SLAM [8] employs the orthonormal representation to parameterize lines and analytically compute the Jacobians, which is the first system to operate the orthonormal re-representation as the minimal parameterize to model lines. BowPL [18] merge ORB-SLAM2

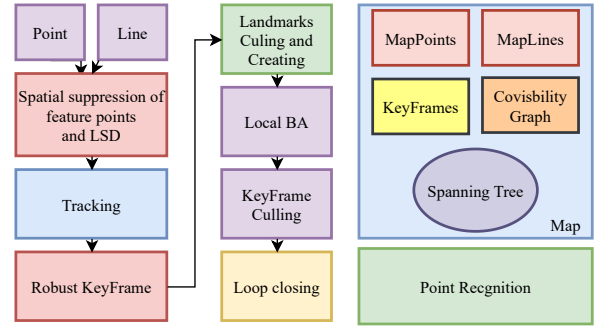


Fig. 2. The architecture of the proposed graph-based visual SLAM system uses fast point, line, and Robust KeyFrame.

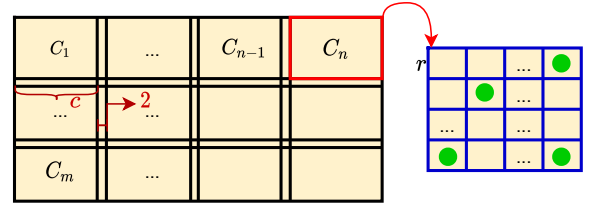


Fig. 3. Feature points were extracted via Spatial suppression with 64 trees.

with PL-SLAM with the Bag-of-words model. To connect broken lines, RPL-SLAM connects lines by points-to-lines distance to improve estimate accuracy. Recent representative works include semi-direct methods about lines and sparse direct methods about the line. Gomez-Ojeda. Propose semi-direct visual odometry(PL-SVO) [19], a two-thread framework that consists of Tracking and Local Mapping with line. It tracks sparse pixels at the FAST corners and lines at LSD to recover motion in Tracking and refines the pose in Local Mapping. SVO uses a depth filter model to estimate pixel depth values and filters outliers

DSO [1] is the direct method, keyframe SLAM system by the pixel's gray value. Regardless of changes in optical flow and exposure parameters under rotation, a new keyframe is created when the weighted sum of optic flow and exposure parameters is greater than 1. The new Keyframe will be used for subsequent sliding window optimization. LSD-SLAM [20] is a large-scale direct monocular SLAM based on Keyframe by change of position.

III. SYSTEM OVERVIEW

Our approach visual SLAM system is based on ORB-SLAM2 and has two different parallel threads see(Fig. 2): Tracking, Local Mapping. Lines are not used to detecting loop place but for global BA. In the following, we briefly describe each component while focusing on the difference between ORB-SLAM2.

A. Spatial suppression of feature points

As shown in Fig. 3, The image consists of multiple cells. The length of the side is set c in each cell. Each cell keeps 2 pixels and has 64 nodes. The Cols of the image are W ,

and The rows of the image are H . Assuming the number of reasonable feature points in this image pyramid is N . n is the number of cols of points, and m is the number of rows of points. Then, considering image resolution, demonstrate the spatial relationship between cols points, rows points, and cells of image computed as follows:

$$\begin{cases} W = c + (n - 1)(\frac{c}{2} + 1) \\ H = c + (m - 1)(\frac{c}{2} + 1), \end{cases} \quad (1)$$

where implies that $N = m \times n$, which the length of side c in each cell is equal to

$$\begin{cases} \delta = 16(N - 1)(W + H + HW - N + 1) \\ \Delta = \sqrt{(W + 2H + 2N + 2)^2 + \delta} \\ c = \frac{-2(W + 2H + 2N + 2) \pm \Delta}{2(N - 1)} \quad (c \geq 64). \end{cases} \quad (2)$$

Restraining the width of the r is used to reduce the number of redundant feature points and is expressed as(3). Only one of most responses for points is an inlier with this width, which we choose to use. Now we have a 64 tree about the length of side c .

$$r = \frac{c}{8} \quad (3)$$

B. Extraction of Line Features

Line Segment detector (LSD) is a commonly used feature to describe line segment texture and is a fast detection method. However, the LSD suffers from the problem of dividing a line into multiple segments [8]. Therefore, this paper attempts to improve the LSD algorithm by mapping image points to Hough space. The center of the image resolution is an origin divided into four quadrants. Therefore, a line l with startpoint $l(x_1, y_1)$ and endpoint $l(x_2, y_2)$. The line of the slope is k , and the line of translation is b as follows:

$$\begin{cases} k = \frac{y_1 - y_2}{x_1 - x_2} \\ b = y_1 - kx_1. \end{cases} \quad (4)$$

From the line in the Hough space, the line is mapped as $l(\rho, \theta)$. The procedure can be expressed as

$$\begin{cases} \theta = -\arctan \frac{1}{k}, & (k < 0, b > 0) \\ \theta = \pi - \arctan \frac{1}{k}, & (k > 0, b > 0), \\ \theta = \pi - \arctan \frac{1}{k}, & (k < 0, b < 0), \\ \theta = 2\pi - \arctan \frac{1}{k}, & (k > 0, b < 0), \\ \rho = x_1 \cos \theta + y_1 \sin \theta. \end{cases} \quad (5)$$

In our approach, we merge the segments according to the same point in Hough space. If ρ smaller than similar line 1% and $\theta < \frac{\pi}{180}$, we fit the straight line through least-squares method with four points. The procedure of fusion is shown in Fig. 4. As our experiments demonstrate, this improved line detector has the advantage of making data associations more

robust and accurate. Note that the merged line segments found by our improved detector is represented by an the LBD line descriptor, which is a 256-bit vector, the same as the ORB point descriptor.

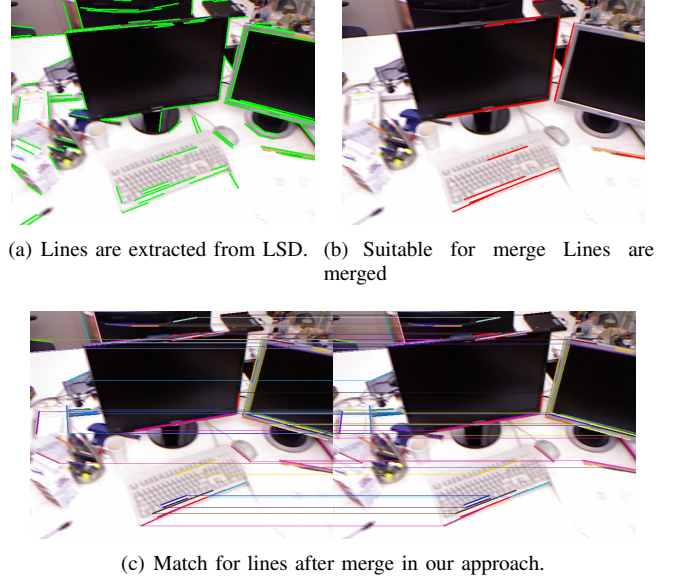


Fig. 4. Results of merge detectors and match.

C. Jacobian of Line Re-projection Error for stereo cameras

Given the extraction of line features, we obtain lines after fitting. we obtain the 2D points p_s and p_e mapping the normalized coordinate system to calculate line function l as follow:

$$l = \frac{p_s \times p_e}{\|p_s\| \|p_e\|}. \quad (6)$$

Then, we formulate the error function based on the point-to-line distance between l and P_l from the matched line. Fig .5 shows the line in the world was observed in three views. The current frame or current keyframe C_{2l} and lats frame or last keyframe C_{1l} present transformation T_{12} . And C_{2l} in left camera for C_{2r} present translation is baseline Bf . Therefore, for each 3D line, the error function can be noted as

$$e_{k,P}^l = \text{III}(R_{k,j}P_l + t_{k,j}). \quad (7)$$

In order to obtain the minimum optimization parameters, the re-projection error of the 3-D line is expressed as the distance

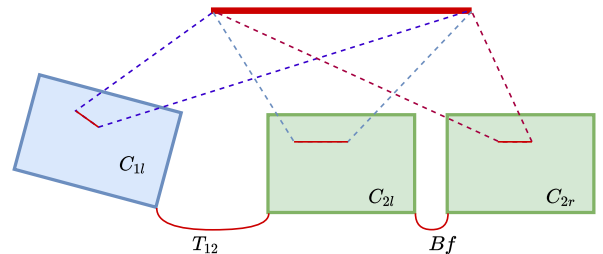


Fig. 5. Line Re-projection Error for stereo cameras to use baseline.

between four homogeneous endpoints. re-projection in left image are $P_{sl}(x_{sl}, y_{sl}, z_{sl})$ and $P_{el}(x_{el}, y_{el}, z_{el})$. right re-projection to left image are $p_{sr}(U_{sr}, \frac{y_{sl}f_y+c_y}{z_{sl}}, 1)$ and $p_{er}(U_{er}, \frac{y_{el}f_y+c_y}{z_{el}}, 1)$ of the matched line segment to the back-projected on image plane as shown in (8).

$$e = \begin{bmatrix} \frac{x_{sl}f_x l_x / z_{sl} + y_{sl}f_y l_y / z_{sl} + l_z}{\sqrt{l_x^2 + l_y^2}} + \frac{x_{el}f_x l_x / z_{el} + y_{el}f_y l_y / z_{el} + l_z}{\sqrt{l_x^2 + l_y^2}} \\ \frac{(U_{sr} + bf / z_{sr})l_x + y_{sr}f_y l_y / z_{sr} + l_z}{\sqrt{l_x^2 + l_y^2}} \\ + \frac{(U_{er} + bf / z_{er})l_x + y_{er}f_y l_y / z_{er} + l_z}{\sqrt{l_x^2 + l_y^2}} \end{bmatrix} \quad (8)$$

Re-project the 3-D point into the current frame, and define the error function based on the re-projection, as shown in the following formula: (9).

$$e_{k,j}^p = p_k - \Pi(R_{k,j}P_j + t_{k,j}) \quad (9)$$

For our method, observations must follow a Gaussian distribution and be independent. The final non-linear least-squares cost T^* can be written as in

$$T^* = \underset{j}{\operatorname{argmin}} \sum_p \rho_p(e_{k,j}^p)^T \Sigma_{pk,j} e_{k,j}^p + \rho_l(e_{k,P_l}^l)^T \Sigma_{pk,P_l} e_{k,j}^l, \quad (10)$$

where $\Sigma_{pk,j}$, $\Sigma_{pk,P}$ are the inverse covariance matrices of points, lines, and ρ_p , ρ_l , are robust Huber cost functions, respectively.

Here, a solution is determined using the Levenberg Marquardt algorithm. It is known that the Jacobian is important when using an iterative approach to solve the graph optimization problem.

In view of (8), we have a error function about the small pose changes $\frac{\partial e}{\partial \delta \zeta}$ as follow:

$$\frac{\partial e}{\partial \delta \zeta} = \frac{\partial e}{\partial l_c} \frac{\partial l_c}{\partial \delta \zeta}. \quad (11)$$

The re-projection error about the lines of cameras pinhole model $\frac{\partial e}{\partial l_c}$.

$$\frac{\partial e}{\partial l_c} = \begin{bmatrix} \frac{f_x l_x}{z \sqrt{l_x^2 + l_y^2}} & \frac{f_y l_y}{z \sqrt{l_x^2 + l_y^2}} & -\frac{x f_y l_y + y f_x l_y}{z^2 \sqrt{l_x^2 + l_y^2}} \\ 0 & \frac{f_y l_y}{z \sqrt{l_x^2 + l_y^2}} & -\frac{b f l_x + y f_y l_y}{z^2 \sqrt{l_x^2 + l_y^2}} \\ 0 & 0 & 0 \end{bmatrix}. \quad (12)$$

Not only do we optimize the poses of the system, but we also optimize landmarks. Therefore, the re-projection error about the lines of landmarks $\frac{\partial e}{\partial P_l}$ can be expressed as (13), where have a rotation matrix $\mathbf{R} \in SO(3)$.

$$\frac{\partial e}{\partial P_l} = \frac{\partial e}{\partial l_c} \mathbf{R} \quad (13)$$

Finally, $\frac{\partial l_c}{\partial \delta \zeta}$ is a jacobian about the small pose changes. The Jacobian of the re-projection error for the small pose changes and landmarks with line parameters can be written as (14) and (15), respectively.

$$j_\zeta = \frac{\partial e}{\partial l_c} \frac{\partial l_c}{\partial \delta \zeta} \quad (14)$$

$$j_P = \begin{bmatrix} \frac{f_x l_x}{z \sqrt{l_x^2 + l_y^2}} & \frac{f_y l_y}{z \sqrt{l_x^2 + l_y^2}} & -\frac{x f_y l_y + y f_x l_y}{z^2 \sqrt{l_x^2 + l_y^2}} \\ 0 & \frac{f_y l_y}{z \sqrt{l_x^2 + l_y^2}} & -\frac{b f l_x + y f_y l_y}{z^2 \sqrt{l_x^2 + l_y^2}} \\ 0 & 0 & 0 \end{bmatrix} \mathbf{R} \quad (15)$$

D. Robust Keyframe

In this way, Robust Keyframe can reduce redundant information. Keyframes below the calculated tracking values between curframe and Keyframe by a certain ratio can be expressed as (16) added. However, the Keyframe of ORB-SLAM2 is poor robustness. we solve the problems to add a offset Δ_{PID} by using PID as Fig .6.

$$KF_{cur} < (KF_{Ref} + \Delta_{PID}) * Ratio. \quad (16)$$

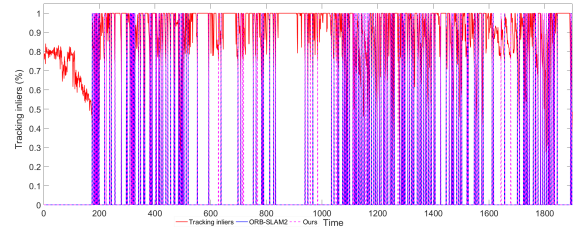


Fig. 6. Comparative results of different methods for selecting keyframes and selecting keyframes in EuRoC V103.

If the point is very far away, the estimation of the position can lead to inaccurate results. The positions between the reference of Keyframe and current Keyframe are used to estimate velocity by way of Kalman filtering.

IV. EXPERIMENTAL RESULTS

System Implementation The Proposed visual SLAM system is based on ORB-SLAM2. Therefore, we describe the main implementation details of my method.

- 1) *Spatial suppression of feature points*: Our system uses a stereo image sequence as input. We use the cv::FAST function for every input frame to extract original features. To eliminate low texture, the threshold was used 7 in function. We set the tolerance value of feature points N to be 0.001. We will return all features to the used estimate state for the setting features more significant than the original features.
- 2) *Line Features*: Four threads are launched to extract point features and line features. Line features are detected by LSD and described by the LBD descriptor. The LSD lines are extracted in zero octaves. Then two threads are launched for stereo matching about lines and points. The endpoints of lines to function are calculated by (6). Then depth values are calculated. Therefore, Matrix information of lines is 0.5 in the Levenberg Marquardt algorithm.
- 3) *Robust Keyframe*: Our system needs to insert Keyframe by PID . Error in PID is calculated between the inliers of the current frame and inliers of the reference frame. $Ratio$ in our method is set to 0.75.

All experiments were carried out with an AMD Ryzen R7-5800H CPU(with @3. 2GHz), NVIDIA GeForce RTX3060

TABLE I
THE TIME FOR KEYPOINTS ALLOCATION IN KITTI AND EUROC DATASETS.

Datasets	MH-01	MH-05	V1-02	V1-03	V2-02	V2-03	KITTI-00	KITTI-01	KITTI-02	KITTI-03	KITTI-04
ORB-SLAM2(ms)	23.79	22.80	25.63	24.07	23.92	66.00	25.33	25.65	16.39	25.91	25.69
Ours(ms)	9.20	7.01	5.92	4.82	6.76	6.27	9.29	8.87	8.68	10.08	9.00

GPU and ubuntu 20. 04. We run each sequence five times and show median results for the accuracy of the estimated trajectory. We evaluate our proposed SLAM system on public datasets and compare its performances with other state-of-the-art methods. The evaluation metrics used in the experiments are the absolute trajectory error (ATE) and the relative pose error (RPE), which measure the absolute and relative pose differences between the estimated and the ground truth motion. The evaluation metrics also include mean tracking time and feature points distributing time.

Evaluation and datasets In order to evaluate our method, we compare it against several stereo SLAM frameworks, as ORB-SLAM2 are state-of-the-art methods. We have also tried to compare our method against Gomez-Ojedas’ PL-SLAM [5], but unfortunately, their approach can not run on our device. To compare our process, we compare our method against another version of Qian’s PL-SLAM. This version is open source and similar to Rubens PL-SLAM. What is more, it is superior to Rubens PL-SLAM. But some datasets also can not run.

In the following, we present the results of Our approach compared to Qians’ PL-SLAM [18] and ORB-SLAM2 in public datasets such as KITTI [21] and EuRoC [22]. Therefore, in this section, PL-SLAM indicates Qians’ PL-SLAM.

A. KeyPoints allocation for time

We evaluate the performance of times in each image pyramid. After the program end, we calculate the time average of all the allocation in each image pyramid. For a fair comparison, in our approach, we set the tolerance value to 0.001, and cv::Fast function for threshold both set 7. Considering the keypoints (ORB) are extracted in an image pyramid with $L = 8$ with a scale ratio of 1.2, our approach is implemented using the same pyramid.

Table I shows the time for keypoints allocation in KITTI and EuRoC datasets. Results show that we obtain the average consumed timeless time to distribute keypoints for each frame than ORB-SLAM2. Fig .7 show the results for distribution from different methods. Results show that our approach presents a well uniform distribution.

B. Pose Estimation and Keyframe numbers

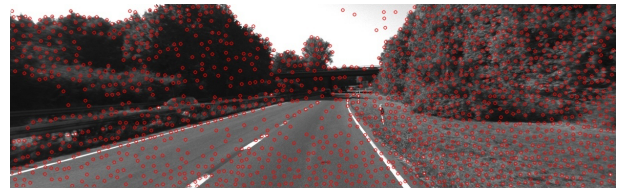
To evaluate our method in different environments, we select the indoor and outdoor datasets, which are EuRoC and KITTI datasets. Note that numbers of lines are 200 in EuRoC datasets and 500 in KITTI datasets. Several open-source approaches are compared in this section, including ORB-SLAM2 and Qians’ PL-SLAM presented in this paper. We evaluate our method’s performance in terms of localization accuracy, computation time, and keyframe numbers. We use $RMSE$ (Root Mean Square Error) of RPE (Relative Pose



(a) The original FAST keypoints.



(b) ORB-SLAM2 FAST keypoints of distribution.



(c) Our FAST keypoints of distribution.

Fig. 7. Comparative results of different distributions for FAST keypoints. Note that in (a), (b), and (c), the green points, the blue points, and the red points indicate the keypoints of position in the frame, respectively.

Error) and ATE (Absolute Trajectory Error) from evo [23] tool. “-” means that the system failed to run the program in the sequence.

EuRoC datasets:All 7 sequences of EuRoC dataset were tested. Results are presented in Table II and Fig .8, respectively. Table II shows the experiment results, where $Trans$ and Rot represent RPE of the translations and rotations, respectively. ATE represents APE of the translations. The $RMSE$ (Table II) shows that ORB-SLAM2 is better than other methods in low drift error in V102-medium and V201-easy to used FAST of low-threshold. Although PL-SLAM has extract lines in a low texture environment, FAST points of low-threshold lead to large drift. Meanwhile, PL-SLAM has a huge time consumption in Fig .9. In addition, PL-SLAM has huge keyframes to finish the program as Fig .8. Huge keyframes indicate low tracking points and lines. Huge keyframes also indicate huge computing power and resources. Our robust method has low drift in ATE . At the same time, our method performs well in RPE of rotation and translation as Table II. ORB-SLAM2 can not extract more texture. Compared to our method, it performs poorly in complex datasets. ORB-SLAM2 runs in V203-difficult as Fig .10 at 14s and 34s. ORB-SLAM2 has a tracking loss. But PL-SLAM and ours can be successfully tracked.10 and shown ORB-SLAM2 has

TABLE II
RESULTS OF ORB-SLAM2, PL-SLAM, AND OURS ON EUROC DATASETS

datasets	ORB-SLAM2			PL-SLAM			Ours		
	ATE(m)	Rot(rad)	Trans(m)	ATE(m)	Rot(rad)	Trans(m)	ATE(m)	Rot(rad)	Trans(m)
MH-04-difficult	0.46	0.0166	0.23	0.67	0.020	0.083	0.21	0.0112	0.069
MH-05-difficult	0.30	0.017	0.075	-	-	-	0.07	0.014	0.061
V1-02-medium	0.064	0.042	0.053	0.064	0.041	0.053	0.067	0.041	0.053
V1-03-difficult	0.13	0.05	0.048	-	-	-	0.11	0.05	0.049
V2-01-easy	0.06	0.02	0.019	0.082	0.02	0.02	0.076	0.0185	0.019
V2-02-medium	0.30	0.046	0.048	-	-	-	0.11	0.043	0.042
V2-03-difficult	1.25	0.18	0.35	1.66	0.11	0.17	0.56	0.079	0.12

poor performance. Our method is more precise. We also demonstrated Fig .9, comparing with time, our method has less time to finish the program than ORB-SLAM2. This method performs better than ORB-SLAM2 2 and PL-SLAM in low texture indoor environments. We have less time to locate and map. In addition, we have higher localization accuracy and smaller keyframes show that our tracking method is robust.

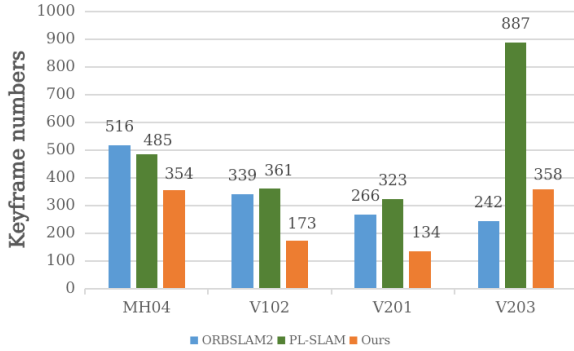
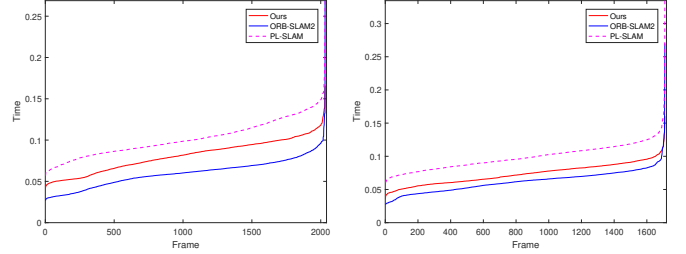


Fig. 8. Keyframe numbers compared with ORB-SLAM2, PL-SLAM, and our method on different sequences on EuRoC.

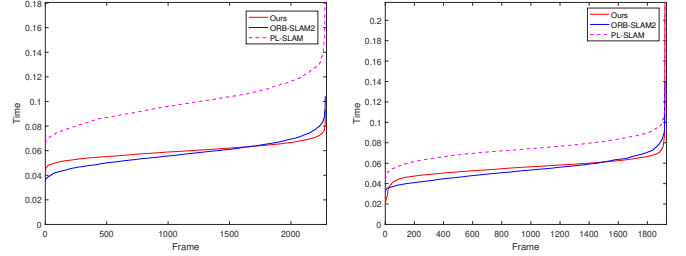
KITTI datasets: Experiments are conducted on all five sequences of KITTI datasets. The KITTI datasets provide large-scale outdoor sequences. We run each sequence three times on our method to have a precision relust.

Table III shows the results of $RMSE$ in the experiment, where $Trans$ and Rot represent RPE of the translations and rotations, respectively. ATE represents APE of the translations. Table III shows that only points SLAM like ORB-SLAM2 will lead to error accumulation. But SLAM has lines that will decrease error. PL-SLAM gets a low drift error as Table III. However, PL-SLAM gets the enormous time that it can not run in real-time, as Fig .11. Our method compared with PL-SLAM, our method track landmark more steady as Fig .11. In Fig .12, our approach takes less time to locate. ORB-SLAM2 has poor performance compared with PL-SLAM and Ours

In Table III, in KITTI-01 datasets, estimation of cameras location has drift due to (17). One point in the world coordinate system is P_w and two frames observe this point in the camera coordinate system named $P_{C1}(X_{C1}, Y_{C1}, Z_{C1})$ and $P_{C2}(X_{C1}, Y_{C1}, Z_{C1})$, respectively. In the camera coordinate $C1$, the camera coordinate $C2$ and the word coordinate W , they have rotation R and translation t for them. Because of far points, the program ignores t . In order to reduce drift, we propose a Kalman algorithm to estimate velocity between



(a) The processing time of a frame on EuRoC MH-04-difficult. (b) The processing time of a frame on EuRoC V1-02-medium.



(c) The processing time of a frame on EuRoC V2-01-easy. (d) The processing time of a frame on EuRoC V2-03-difficult

Fig. 9. The processing time of a frame on EuRoC. Noted that red is our method, pink is PL-SLAM, and blue is ORB-SLAM for the processing time.

referenced Keyframe and the current frame. The camera's velocity can be greater than $7m/s$ will add keyframes. This way, we can do multiple estimates to reduce ignoring t .

$$\begin{bmatrix} X_{C1} \\ Y_{C1} \\ Z_{C1} \end{bmatrix} = \mathbf{R} \begin{bmatrix} X_{C2} \\ Y_{C2} \\ Z_{C2} \end{bmatrix} + \mathbf{t}. \quad (17)$$

In Fig .13, the result shows our method has localization accuracy greater than ORB-SLAM2 and PL-SLAM. ORB-SLAM2 use far points to estimate state, leading to a vast error translation of around $5.56m$ on ATE . PL-SLAM tries to use lines to reduce error translation but shows the extensive time as Fig .11. Our method solves the problem with lines and keyframes between the Kalman algorithm and PID leading to less time and fewer keyframes as Fig11. Fig14 shows our system's effect on the KITTI-01 dataset . Our system connects disconnected segments to create a better mapping than PL-SLAM.

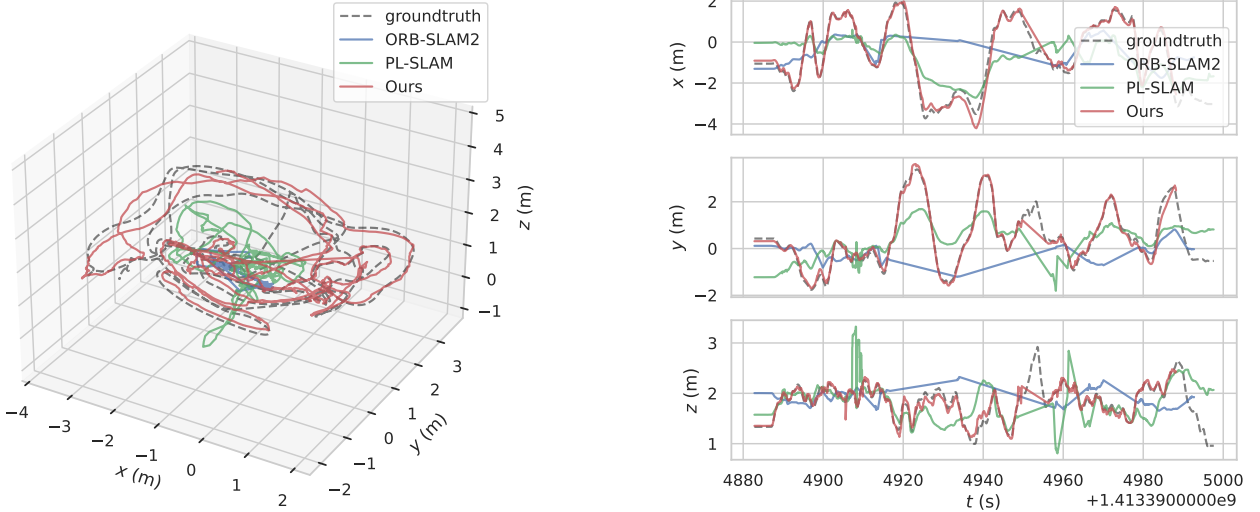


Fig. 10. Localization accuracy comparison of our method with ORB-SLAM2 and PL-SLAM. The left results show the 3D motion trajectories, and the right results show trajectories with 2D.

TABLE III
RESULTS OF ORB-SLAM2, PL-SLAM, AND OURS ON KITTI DATASETS.

datasets	ORB-SLAM2			PL-SLAM			Ours		
	ATE(m)	Rot(rad)	Trans(m)	ATE(m)	Rot(rad)	Trans(m)	ATE(m)	Rot(rad)	Trans(m)
KITTI-01	5.56	0.0009	0.049	3.73	0.021	0.05	3.21	0.0007	0.046
KITTI-03	0.42	0.0009	0.017	-	-	-	0.31	0.001	0.017
KITTI-04	0.18	0.0007	0.02	0.16	0.0006	0.02	0.21	0.0009	0.022
KITTI-05	0.42	0.001	0.016	0.38	0.0009	0.016	0.87	0.002	0.024
KITTI-06	0.90	0.0008	0.033	0.82	0.0007	0.018	0.73	0.0009	0.017

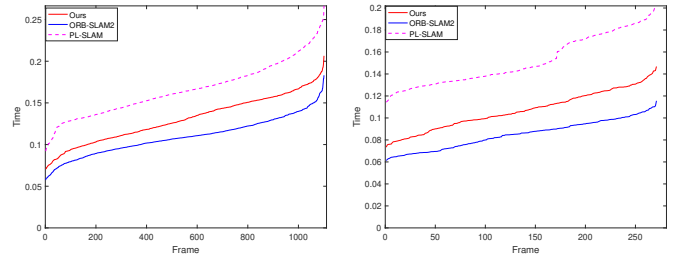
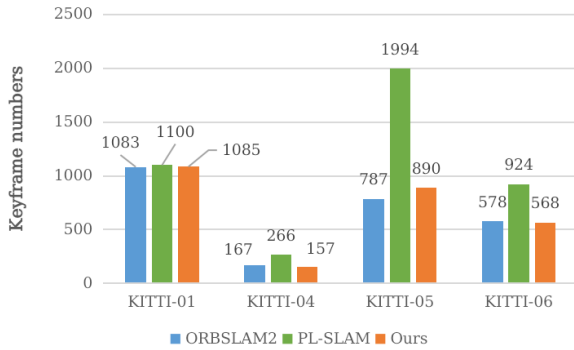
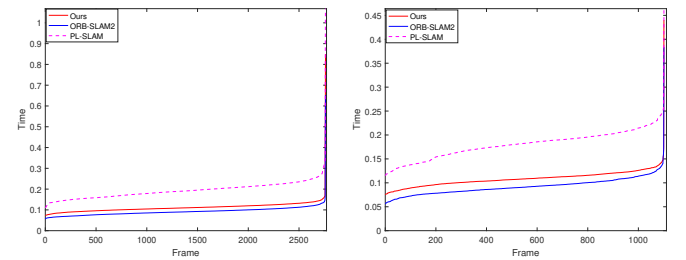


Fig. 11. Keyframe numbers in comparison with ORB-SLAM2, PL-SLAM, and our method on different sequences(left) on KITTI and a comparison of average runtime for one of the input frames(right) on KITTI.

(a) The processing time of a frame on KITTI-01. (b) The processing time of a frame on KITTI-04.

V. CONCLUSIONS

To improve the accuracy and robustness of visual SLAM, we present a graph-based approach using spatial suppression of feature points and line features with baseline and robust keyframe on *PID* and Kalman algorithm. Suppression of feature points takes less time to finish the system in a lower threshold value on FAST. The Jacobians of re-projection error concerning the line parameters consider baseline making a good performance. And *PID* keyframe and Kalman keyframe wise decisions to insert keyframes. They demonstrated that the fusion baseline lines produces more robust estimations in real-world scenarios. In the future, we will study how to introduce



(c) The processing time of a frame on KITTI-05. (d) The processing time of a frame on KITTI-06.

Fig. 12. The processing time of a frame on KITTI. Noted that red is our method, pink is PL-SLAM, and blue is ORB-SLAM for the processing time.

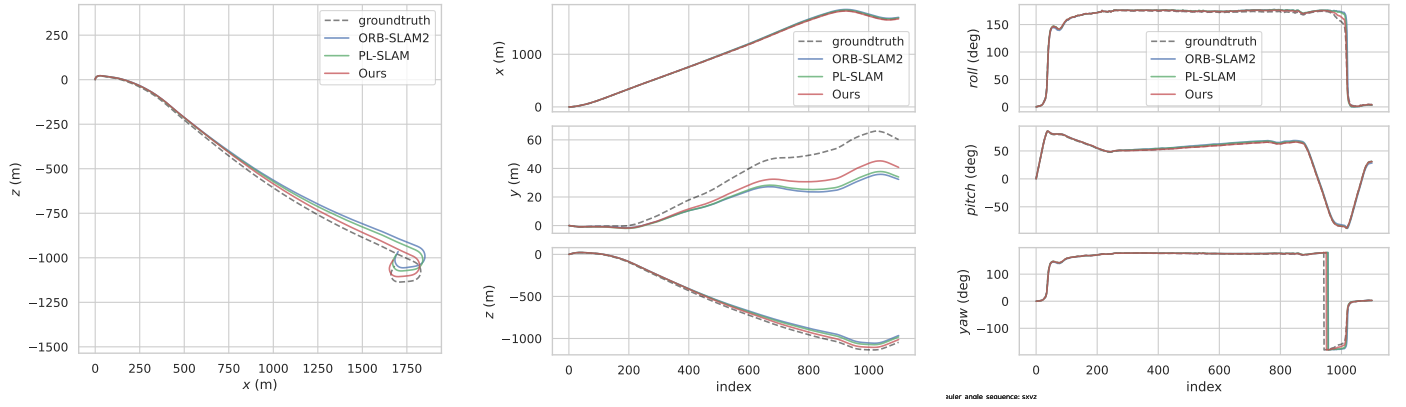


Fig. 13. Localization accuracy comparison of our method with ORB-SLAM2 and PL-SLAM without $SE(3)$ Umeyama. Left cols of results show 3D trajectories on xz coordinate system, the second results show translations of trajectories, and the last results show the rotation of trajectories.

$$j_{\zeta} = \begin{bmatrix} \frac{f_x l_x}{z\sqrt{l_x^2+l_y^2}} & \frac{f_y l_y}{z\sqrt{l_x^2+l_y^2}} & -\frac{f_x l_x+f_y l_y y}{z^2\sqrt{l_x^2+l_y^2}} & -\frac{f_x l_x y-f_y l_y y^2}{z^2\sqrt{l_x^2+l_y^2}} & -\frac{f_y l_y}{\sqrt{l_x^2+l_y^2}} & \frac{x f_x l_x+f_y l_y x y}{z^2\sqrt{l_x^2+l_y^2}} + \frac{f_x l_x}{\sqrt{l_x^2+l_y^2}} & \frac{f_y l_y x-f_x l_x y}{z\sqrt{l_x^2+l_y^2}} \\ 0 & \frac{f_y l_y}{z\sqrt{l_x^2+l_y^2}} & -\frac{b f l_x-f_y l_y y}{z^2\sqrt{l_x^2+l_y^2}} & -\frac{y b f l_x+f_y l_y y^2}{z^2\sqrt{l_x^2+l_y^2}} & -\frac{f_y l_y}{\sqrt{l_x^2+l_y^2}} & \frac{x b f l_x+f_y l_y x y}{z^2\sqrt{l_x^2+l_y^2}} & \frac{f_y l_y x}{z\sqrt{l_x^2+l_y^2}} \\ 0 & 0 & 0 & 0 & 0 & 0 & 0 \end{bmatrix} \quad (18)$$

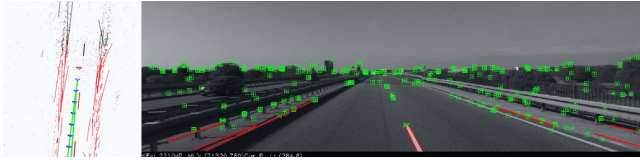


Fig. 14. The proposed visual SLAM with point and line features on our program on KITTI-01.

inertial sensors into our system with point and line features.

In view of (14), the Jacobian of the re-projection error with line parameters in detail show at (18).

REFERENCES

- [1] R. Wang, M. Schworer, and D. Cremers, "Stereo dso: Large-scale direct sparse visual odometry with stereo cameras," in *Proceedings of the IEEE International Conference on Computer Vision*, pp. 3903–3911, 2017.
- [2] C. Forster, M. Pizzoli, and D. Scaramuzza, "Svo: Fast semi-direct monocular visual odometry," in *2014 IEEE international conference on robotics and automation (ICRA)*, pp. 15–22, IEEE, 2014.
- [3] R. Mur-Artal and J. D. Tardós, "Orb-slam2: An open-source slam system for monocular, stereo, and rgb-d cameras," *IEEE transactions on robotics*, vol. 33, no. 5, pp. 1255–1262, 2017.
- [4] A. Pumarola, A. Vakhitov, A. Agudo, A. Sanfeliu, and F. Moreno-Noguer, "Pl-slam: Real-time monocular visual slam with points and lines," in *2017 IEEE international conference on robotics and automation (ICRA)*, pp. 4503–4508, IEEE, 2017.
- [5] R. Gomez-Ojeda, F.-A. Moreno, D. Zuniga-Noël, D. Scaramuzza, and J. Gonzalez-Jimenez, "Pl-slam: A stereo slam system through the combination of points and line segments," *IEEE Transactions on Robotics*, vol. 35, no. 3, pp. 734–746, 2019.
- [6] S. Buoncompagni, D. Maio, D. Maltoni, and S. Papi, "Saliency-based keypoint selection for fast object detection and matching," *Pattern Recognition Letters*, vol. 62, pp. 32–40, 2015.
- [7] Y. Li, N. Brasch, Y. Wang, N. Navab, and F. Tombari, "Structure-slam: Low-drift monocular slam in indoor environments," *IEEE Robotics and Automation Letters*, vol. 5, no. 4, pp. 6583–6590, 2020.
- [8] X. Zuo, X. Xie, Y. Liu, and G. Huang, "Robust visual slam with point and line features," in *2017 IEEE/RSJ International Conference on Intelligent Robots and Systems (IROS)*, pp. 1775–1782, IEEE, 2017.
- [9] Y. Li, R. Yunus, N. Brasch, N. Navab, and F. Tombari, "Rgb-d slam with structural regularities," in *2021 IEEE International Conference on Robotics and Automation (ICRA)*, pp. 11581–11587, IEEE, 2021.
- [10] H. Strasdat, J. Montiel, and A. J. Davison, "Scale drift-aware large scale monocular slam," *Robotics: Science and Systems VI*, vol. 2, no. 3, p. 7, 2010.
- [11] R. G. Von Gioi, J. Jakubowicz, J.-M. Morel, and G. Randall, "Lsd: a line segment detector," *Image Processing On Line*, vol. 2, pp. 35–55, 2012.
- [12] S.-S. Huang, Z.-Y. Ma, T.-J. Mu, H. Fu, and S.-M. Hu, "Lidar-monocular visual odometry using point and line features," in *2020 IEEE International Conference on Robotics and Automation (ICRA)*, pp. 1091–1097, IEEE, 2020.
- [13] Q. Jiang, M. Liu, X. Wang, M. Ge, and L. Lin, "Human motion segmentation and recognition using machine vision for mechanical assembly operation," *SpringerPlus*, vol. 5, no. 1, pp. 1–18, 2016.
- [14] G. Klein and D. Murray, "Parallel tracking and mapping on a camera phone," in *2009 8th IEEE International Symposium on Mixed and Augmented Reality*, pp. 83–86, IEEE, 2009.
- [15] Q. Fu, H. Yu, X. Wang, Z. Yang, Y. He, H. Zhang, and A. Mian, "Fastorb-slam: Fast orb-slam method with descriptor independent keypoint matching," *arXiv preprint arXiv:2008.09870*, 2020.
- [16] O. Bailo, F. Rameau, K. Joo, J. Park, O. Bogdan, and I. S. Kweon, "Efficient adaptive non-maximal suppression algorithms for homogeneous spatial keypoint distribution," *Pattern Recognition Letters*, vol. 106, pp. 53–60, 2018.
- [17] L. Zhang and R. Koch, "An efficient and robust line segment matching approach based on lbd descriptor and pairwise geometric consistency," *Journal of Visual Communication and Image Representation*, vol. 24, no. 7, pp. 794–805, 2013.
- [18] K. Qian, W. Zhao, K. Li, X. Ma, and H. Yu, "Visual slam with boplw pairs using egocentric stereo camera for wearable-assisted substation inspection," *IEEE Sensors Journal*, vol. 20, no. 3, pp. 1630–1641, 2019.
- [19] R. Gomez-Ojeda, J. Briales, and J. Gonzalez-Jimenez, "Pl-svo: Semi-direct monocular visual odometry by combining points and line segments," in *2016 IEEE/RSJ International Conference on Intelligent Robots and Systems (IROS)*, pp. 4211–4216, IEEE, 2016.
- [20] J. Engel, T. Schöps, and D. Cremers, "Lsd-slam: Large-scale direct monocular slam," in *European conference on computer vision*, pp. 834–849, Springer, 2014.
- [21] A. Geiger, P. Lenz, and R. Urtasun, "Are we ready for autonomous driving? the kitti vision benchmark suite," in *Conference on Computer Vision and Pattern Recognition (CVPR)*, 2012.
- [22] M. Burri, J. Nikolic, P. Gohl, T. Schneider, J. Rehder, S. Omari, M. W. Achtelik, and R. Siegwart, "The euroc micro aerial vehicle datasets," *The International Journal of Robotics Research*, 2016.
- [23] M. Grupp, "Python package for the evaluation of odometry and slam," 2017.